Internal strain drives spontaneous periodic buckling in collagen and regulates remodeling

Andrew Dittmore[a], Jonathan Silver[a], Susanta K. Sarkar[a], Barry Marmer[b], Gregory I. Goldberg[b,1], and Keir C. Neuman[a,1]

[a]Laboratory of Single Molecule Biophysics, National Heart, Lung and Blood Institute, National Institutes of Health, Bethesda, MD 20892; and [b]Division of Dermatology, Department of Medicine, Washington University School of Medicine, Saint Louis, MO 63130

Edited by Steven M. Block, Stanford University, Stanford, CA, and approved June 1, 2016 (received for review November 24, 2015)

Fibrillar collagen, an essential structural component of the extracellular matrix, is remarkably resistant to proteolysis, requiring specialized matrix metalloproteinases (MMPs) to initiate its remodeling. In the context of native fibrils, remodeling is poorly understood; MMPs have limited access to cleavage sites and are inhibited by tension on the fibril. Here, single-molecule recordings of fluorescently labeled MMPs reveal cleavage-vulnerable binding regions arrayed periodically at ∼1-μm intervals along collagen fibrils. Binding regions remain periodic even as they migrate on the fibril, indicating a collective process of thermally activated and self-healing defect formation. An internal strain relief model involving reversible structural rearrangements quantitatively reproduces the observed spatial patterning and fluctuations of defects and provides a mechanism for tension-dependent stabilization of fibrillar collagen. This work identifies internal-strain-driven defects that may have general and widespread regulatory functions in self-assembled biological filaments.

collagenase | matrix metalloproteinase | single molecule | pattern formation | mechanosensing

Collagen comprises over 30% of the protein mass of the human body and is an abundant structural protein in all animals (1). In its most common form, fibrillar collagen assembles from ∼300-nm polypeptide triple helices (tropocollagen) into highly organized, hierarchical networks that provide the protein scaffolding for the extracellular matrix, tendons, bones, and other load-bearing structures (1–3). The triple helix is highly resistant to proteolysis and collagen degradation requires a specialized class of proteases called matrix metalloproteinases (MMPs) (1, 4–6). Only four of the 23 human MMPs can initiate degradation of fibrillar collagen (6, 7). They cleave all three polypeptide chains of tropocollagen asynchronously at a unique thermally labile site located ∼225 nm from the N terminus (8, 9). MMPs play important physiological roles during development and wound healing, promoting cell motility, angiogenesis, and tissue remodeling (6, 10–12). MMP activity is regulated through gene expression and through binding of specific tissue inhibitors of metalloproteinase (13, 14). In addition, MMP activity is regulated by mechanical stress on fibrillar collagen, which inhibits proteolysis through an unknown mechanism (15–17). Dysregulation of MMP activity is implicated in rheumatoid arthritis, atherosclerosis, tumor progression, and metastasis (13, 18, 19).

Despite the importance of collagen remodeling for human health and disease, the mechanistic details of how MMPs degrade fibrillar collagen are not well established. Physiologically relevant collagen fibrils are heterogeneous and insoluble filamentous protein assemblies that are refractory to conventional biochemical analysis (20), yet a spatially extended substrate permits measurements of MMPs moving on fibrillar collagen through fluorescence correlation spectroscopy (20–22) and, more recently, direct single-molecule tracking (23). These studies revealed that MMPs undergo one-dimensional diffusion on the fibril, frequently interrupted by transient binding. Degradation initiates from a small subset of binding events; MMP then executes ∼15 or more cleavage reactions in rapid succession resulting in processive bursts of motion along the fibril. Processive and directional MMP cleavage is consistent with structural models of fibrillar collagen proposed by Orgel and coworkers (2, 5, 23) in which tropocollagen is assembled into an oriented microfibrillar structure with MMP cleavage sites spaced at regular 67-nm intervals (the D period) and covered by the C-terminal end of the preceding triple helix.

The initial cleavage event is a key step in the MMP regulation pathway that warrants further consideration. First, in static structural models of fibrillar collagen, cleavage sites are inaccessible to MMP due to the molecular packing architecture (2, 5). Second, statistical analysis of the relative MMP binding positions preceding proteolysis suggested a highly regular spatial periodicity of ∼1 μm, but the origin of these privileged entry sites is unknown (23). Here, by performing high-resolution single-molecule tracking of MMPs over long periods of time, we directly show MMP binding sites arrayed at ∼1-μm intervals along individual collagen fibrils. Remarkably, the binding sites slowly migrate along the collagen fibril while the large-scale pattern remains periodic. This behavior can be explained by an internal strain model in which binding sites correspond to regions of local defect formation that relieve internal strain within the fibril. This model captures the periodicity and fluctuations of the binding regions and provides a mechanistic description of how MMPs gain access to the otherwise inaccessible cleavage sites in fibrillar collagen. The internal strain model provides an elegant mechanism through which external strain inhibits MMP degradation of fibrillar collagen by eliminating the spontaneous formation of defects.

High-Affinity MMP-1 Binding Regions on Fibrillar Collagen Are Periodic and Dynamic

To determine the pattern of interactions of MMPs with native fibrillar collagen and gain insight into the initiation mechanism, we mapped the binding positions of thousands of individual MMP enzymes with high temporal and spatial resolution. We used total internal reflection fluorescence (TIRF) microscopy to

Significance

Collagen fibrils resemble nanoscale cables that self-assemble and constitute the most prevalent protein structure in the body. Our experiments reveal unanticipated defects that form along collagen fibrils. These defects are the initiation sites of collagenase activity and represent a strain-sensitive mechanism for regulating tissue remodeling. The emergence of defects, their spatial periodicity, and fluctuations are quantitatively accounted for with a buckling model in which defects spontaneously form, repulsively interact, and self-heal.

Author contributions: A.D., S.K.S., B.M., G.I.G., and K.C.N. designed research; A.D., J.S., S.K.S., B.M., and G.I.G. performed research; A.D., J.S., B.M., G.I.G., and K.C.N. contributed new reagents/analytic tools; A.D., J.S., G.I.G., and K.C.N. analyzed data; and A.D., J.S., G.I.G., and K.C.N. wrote the paper.

The authors declare no conflict of interest.

This article is a PNAS Direct Submission.

Freely available online through the PNAS open access option.

[1]To whom correspondence may be addressed. Email: neumankc@mail.nih.gov or goldberg@medicine.wustl.edu.

This article contains supporting information online at www.pnas.org/lookup/suppl/doi:10.1073/pnas.1523228113/-/DCSupplemental.

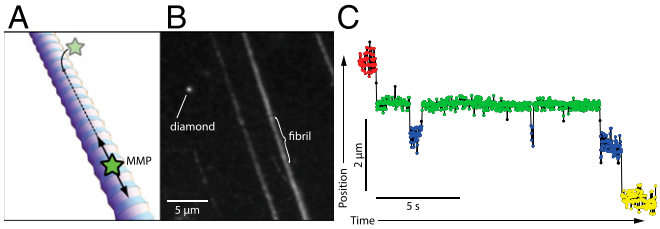

Fig. 1. Single-molecule tracking of MMP on fibrillar collagen. (*A*) Cartoon of experimental geometry (not to scale) depicting collagen fibril with 67-nm periodic axial banding (D period). Collagen remodeling enzymes (MMPs) (green star) bind and diffuse on the fibril. (*B*) Experimental geometry used for single-molecule enzyme tracking. Type I rat tail collagen fibrils were bound to a quartz slide and fluorescently labeled MMPs were visualized with TIRF microscopy. A fluorescent nanodiamond was used to correct for stage drift. (*C*) Example single-molecule trajectory depicting the position of the MMP along the collagen fibril as a function of time. As the MMP moves along the fibril, it dwells in well-separated binding regions, which are indicated by different colors. The spatial extent of the dwells (~0.25 μm, full width at half maximum) exceeds the tracking uncertainty (~40 nm at 10-ms exposure).

record fluorescently tagged MMP molecules binding to the surface of native type I collagen fibrils (Fig. 1*A*) (23). To avoid potential complications from fibril degradation, we initially used an MMP-1 construct harboring an E219Q point mutation (mutMMP-1); this enzyme binds and diffuses but does not cleave the fibril (24, 25). Individual mutMMP-1 molecules diffuse in one-dimensional tracks along the fibril and dwell in well-defined binding regions (Fig. 1*C* and Figs. S1 and S2*A*) from which active MMP-1 initiates degradation (23).

Simultaneous tracking of mutMMP-1 molecules over 2 min (Fig. 2*A*) reveals that, on short timescales (~2 s), different enzymes sequentially bind to the same regions on the fibril. As one mutMMP-1 molecule escapes from a binding region, it is rapidly replaced by another enzyme that binds at the same region. Moreover, enzymes that diffuse away from a binding region but remain attached to the fibril invariably bind to the adjacent high-affinity binding site (Fig. 2*A*). Together, these observations indicate that the high-affinity binding regions represent a feature of the collagen fibril independent of individual MMPs. We therefore combined the binding positions of individual enzymes in overlapping 1-s intervals spaced by 0.2 s to precisely locate the center of each binding region by Gaussian fitting (Fig. 2 *B*–*D*). The resulting high-resolution map of binding sites over time establishes that the binding regions are persistent features periodically arrayed on the fibril with an unanticipated ~1-μm length scale, significantly longer than the ~300-nm monomer length or 67-nm D period.

Similar binding site periodicity was observed for active MMP-1, the prototypical collagenase, and for MMP-9, a gelatinase, demonstrating that spatially periodic binding is not enzyme-specific and lending further support to the conclusion that the binding sites correspond to structural changes in the fibrillar substrate (Fig. 3). Furthermore, similar periodicity observed after a high-salt wash or trypsin digestion of the collagen fibrils indicates that patterning is independent of ancillary proteins, which are removed by these treatments (Fig. 3).

On longer timescales (~20 s), the binding sites were observed to be dynamic (Movie S1 and Fig. S2*B*); they randomly move along fibrils and are occasionally spontaneously created or annihilated (Fig. 4*A*). One binding site can split into two, or two sites can merge into one (Fig. 4*A*). To capture these slow binding site dynamics, we extended the tracking measurements over 20 min (Fig. 4*B*). Strikingly, the binding sites maintained ~1-μm periodicity (Fig. 4*F*) but the entire periodic pattern slowly reorganized, as evidenced by the shift between spatially periodic patterns separated by 18 min (Fig. 4 *B* and *C*) and the essentially uniform distribution of dwell positions on the fibril over the entire 20-min period (Fig. 4*D*). The time evolution of the binding pattern is characterized by two exponential timescales (Fig. 4*E*): $\tau_1 = 1.4 \pm 0.2$ s, corresponding to locally constrained motion of binding sites (Fig. S2*B*), and $\tau_2 = 18 \pm 4$ s, corresponding to more gradual rearrangements such as binding sites splitting and merging. These dynamic features indicate that the binding regions correspond to reversible structural fluctuations of the fibril.

An expanded 2D localization map of two binding regions corresponding to mutMMP-1 dwell positions at different times (Fig. 4*G*) reveals that individual dwells occur at random lateral positions across the ~100-nm fibril. The lateral spread of dwell positions indicates that individual enzymes bind on different parallel tracks (26), and that binding regions extend in bands around the fibril.

Internal–Strain-Dependent Defect Formation Model of Periodic Binding Regions

The data indicate that dynamic structural fluctuations occur spontaneously with a periodicity of ~1 μm and that this periodicity is preserved even as the structural defects migrate over the surface of the collagen fibril. To understand the mechanistic origin of this behavior, we focused on the periodicity, which is

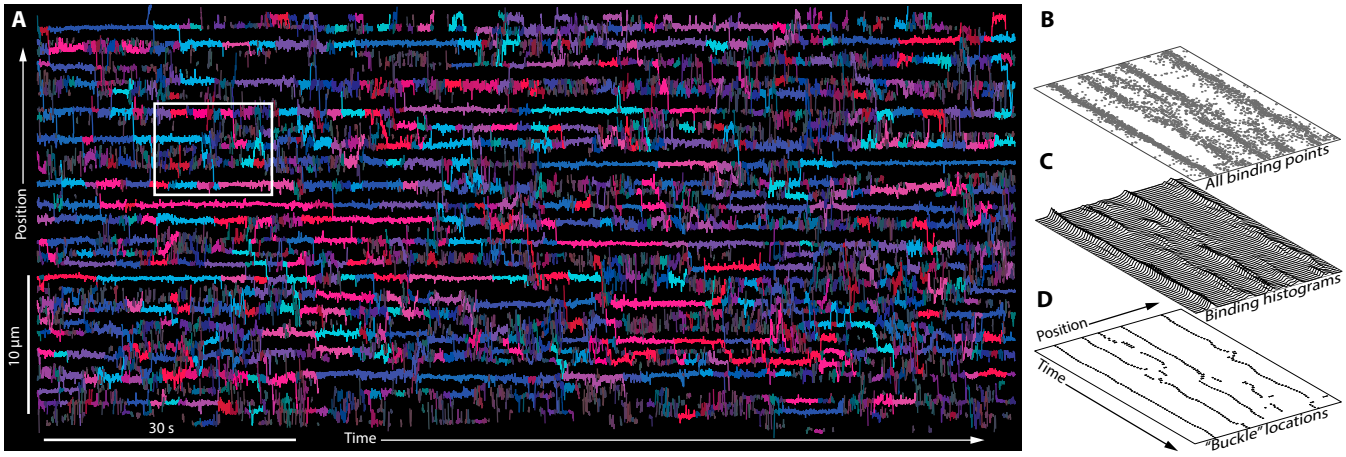

Fig. 2. Mapping of collagen fibril binding locations from individual MMP trajectories. (*A*) Plot of MMP positions along the fibril as a function of time for hundreds of single molecules. Each continuous colored line corresponds to the trajectory of a single MMP. Long trajectories are colored more brightly. Colors are repeated for different molecules. (*B*) MMP binding data from the boxed region of *A*. (*C*) Histogram of binding positions from *B* over a sliding 1-s window updated every 0.2 s. (*D*) Location of MMP binding regions determined from the positions of peaks in *C*. Error bars equal to the SEM determined by Gaussian fitting are similar to the point size. Additional details are provided in *Supporting Information*.

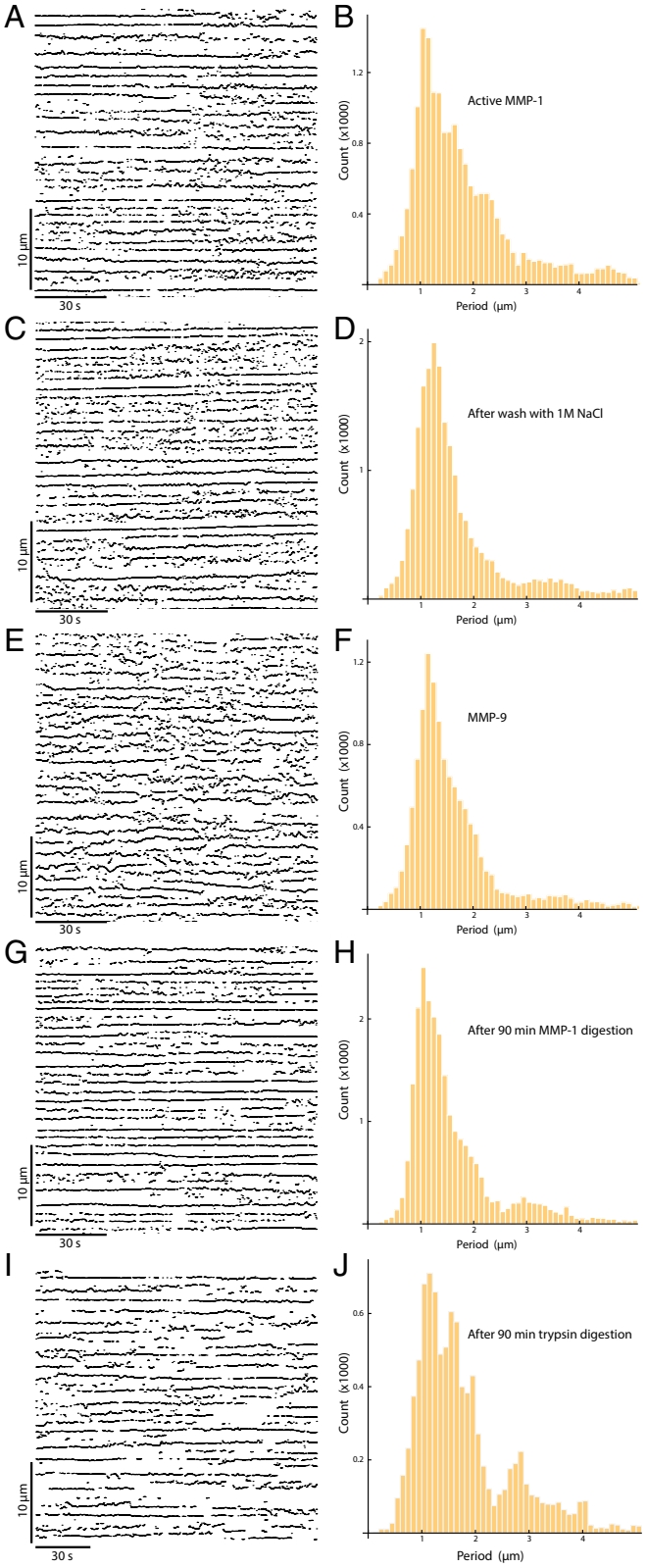

Fig. 3. Micrometer-scale periodicity of binding sites observed with different MMP constructs and different fibrils subjected to treatments to remove bound proteins: (*A* and *B*) active wild-type MMP-1, the prototypical collagenase; (*C* and *D*) active wild-type MMP-1 after washing with 1 M NaCl to remove nonspecifically bound proteins; (*E* and *F*) active wild-type MMP-9, a gelatinase; (*G* and *H*) mutant MMP-1 (E219Q) after 90 min of digestion with active MMP-1; and (*I* and *J*) active wild-type MMP-1 after 90 min of trypsin digestion, which degrades noncollagen proteins bound to the fibril. The periodicity is similar under all conditions. *A*, *C*, *E*, *G*, and *I* are spatiotemporal maps of binding regions similar to Figs. 2*D* and 4*A*. *B*, *D*, *F*, *H*, and *J* are histograms of the distances between adjacent binding regions at each time step (0.2 s) for the spatiotemporal maps in *A*, *C*, *E*, *G*, and *I*.

reminiscent of spatial patterns formed as a result of internal strain such as those found in cracking mud or pottery glazes, at the interface of incommensurate crystal lattices, or in the buckling patterns of thin films (27–29). Inspired by these examples of local internal strain relief leading to large-scale spatial patterning, we developed a mechanistic model (Fig. 5) that reproduces the essential features of the experimental data. The essence of the model is that two distinct structural phases of collagen coexist that are distinguished by the degree of mechanical strain. In the "intact" phase, collagen monomers are forced into a straight conformation maintained by lateral contacts (30), resulting in the accumulation of internal strain. In the "alternate" phase, strain is relieved by the formation of "buckled" molecular configurations where MMP is assumed to bind preferentially due to the exposure of collagen cleavage sites in the buckled region. The disruption of lateral contacts in a buckled region is assumed to occur reversibly and cooperatively in a band around the fibril, resulting in a one-dimensional model. Additional support for this model is provided by recent observations of micrometer-scale periodic regions of reduced elastic modulus along collagen fibrils, which are consistent with the formation of locally buckled or otherwise structurally altered sites (31) (Fig. S3).

In order for binding regions to emerge spontaneously, their formation must lower the free energy of the system. A fibril entirely in the intact phase would be in a high-energy state due to the internal mechanical strain indicated by the area under the uniform strain energy density curve (dotted line in Fig. 5*A*). In the region of a buckle, strain is relieved. In a linear approximation, the strain energy density drops to a minimum at the center of the buckle and returns to the baseline value over a distance $w/2$, defining a triangle-shaped area of strain energy relief (Fig. 5*A* and Fig. S4). We assume that formation of a buckle involves a structural transition with free energy cost μ. If the strain energy relief associated with buckling exceeds μ, buckles spontaneously form, lowering the total energy. The buckling process is self-limiting because, as the number of buckles n increases, the average strain reduction per buckle (calculated from the area between the energy density curves) decreases as the strain relief areas of neighboring buckles begin to overlap (Fig. 5*A*). The buckles effectively repel each other when they get closer together than w. The repulsive force between buckles, calculated from the change in strain energy with interbuckle separation x, is $k(w-x)$, $(x<w)$, characterized by the effective spring constant k. The energy is lowest for evenly distributed buckles with spacing $\bar{x}$, but, if the characteristic energy scales are on the order of thermal energy, the number and spacing of buckles will fluctuate subject to thermal noise (*Methods*).

The key parameters of the model can be extracted from the experimental data. The effective spring constant is related to the variance of the distances between adjacent binding regions, σ_x^2, by $k=k_BT/\sigma_x^2$, where k_B is Boltzmann's constant and T is the absolute temperature. We estimate $k=12.3\pm0.8\ k_BT/\mu m^2$ ($\approx 5\times10^{-8}$ N/m) from the observed variance (Fig. 4*F*). The energy of buckle formation, $\mu=k\bar{x}^2/2$, returns an estimate of $\mu=7.7\pm0.5\ k_BT$. The fact that μ is a small multiple of thermal energy means that thermal fluctuations are sufficient to cause binding regions to spontaneously form and disappear, consistent with the observed dynamics (Fig. 4). Monte Carlo simulations of the model recapitulate the essential features of spatial patterning (Fig. 5*C*). Using the spring constant k and buckling energy μ as input parameters, we recorded the distributions of the number of buckles, n, over 10.7 μm and distance between buckles, x, after a number of simulation steps calculated to generate uncorrelated configurations (*Methods*). Independent of the initial buckle number or configuration, the simulation reached a steady state with reproducible number and interbuckle distance

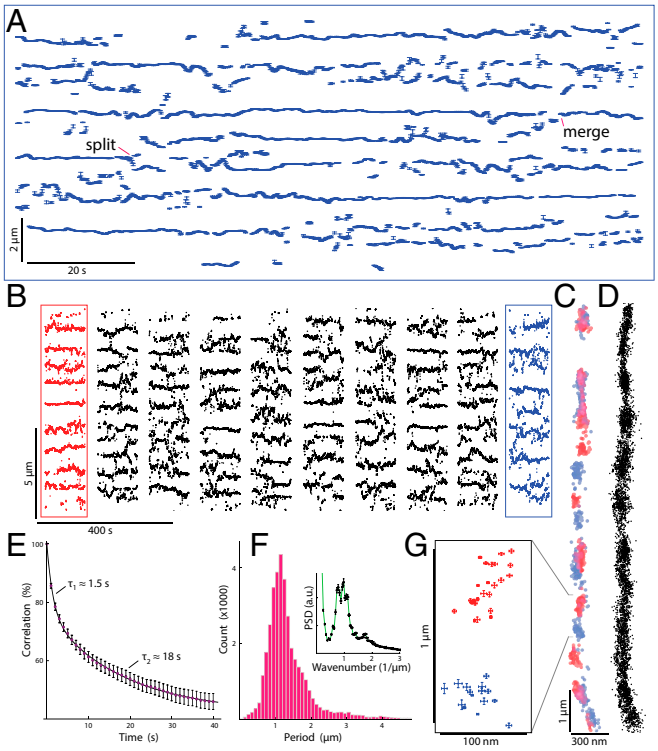

Fig. 4. Binding regions in fibrillar collagen are periodic and dynamic. (*A*) Spatiotemporal map of collagen binding sites as calculated in Fig. 2*D*. Positions of individual binding regions persist over several tens of seconds with rough spatial periodicity. However, the sites move locally, and the number of binding sites changes occasionally through spontaneous creation (split) and annihilation (merge) events. (*B*) Map of binding site locations from more than 30,000 single-molecule trajectories plotted as a function of time. Positions along the fibril were measured with reference to the stable diamond fiducial marker. Gaps in the data set indicate breaks in the recording when enzyme was replenished in the sample chamber. (*C*) Single-molecule localization of binding events. Each point marks the mean position in two dimensions of an individual MMP molecule dwelling in a binding region for more than 0.2 s. Colors correspond to single-enzyme events in the first (red) and last (blue) portions in the data set in *B* and are darker where points overlap. The scale across the fibril is 3× the scale along the fibril. (*D*) Single-molecule localization of binding events over the full data set. (*E*) Correlation times of the periodic binding pattern fit with a sum of exponentials with decay times $\tau_1 = 1.4 \pm 0.2$ s and $\tau_2 = 18 \pm 4$ s (*Supporting Information*). (*F*) Histogram of the distances between adjacent binding regions at each time step (0.2 s) for the data in *B*. The peak indicating the dominant spatial periodicity of 1.12 ± 0.01 μm is also evident in the power spectral analysis of the binding patterns along the fibril (*Inset* and *Supporting Information*). (*G*) Detail of single-molecule localization from *C* for molecules that dwelled within a binding region for more than 1 s. Error bars are the SEM. The scale across the fibril is 3× the scale along the fibril axis.

distributions (Fig. S5). Features such as the overall periodicity, movement of buckles, bifurcations, and merging events observed experimentally (Figs. 3 and 4) are reproduced in the simulations (Fig. 5*C*).

Possible Influence of Boundary Conditions on Dynamic Rates

Covalent surface attachment was necessary to obtain stable, absolute position measurements but could affect the pattern dynamics. Attachment to the surface interrupts the continuity of the fibril circumference and might cause local distortions that could alter the dynamics of buckling. In a similar vein, we note that enzyme binding could also affect dynamics by stabilizing the buckled state. Whereas such perturbations could impact the correlation timescales reported in Fig. 4*E* and Fig. S2*B*, multiple lines of evidence indicate that the underlying buckling phenomenon is independent of these perturbations: (*i*) If buckling were caused by the surface attachment, then the buckle pattern would be expected to be static and heterogeneous. However, the buckling patterns are, in fact, dynamic and, over time, are homogeneously distributed along the fibril (Fig. 4*D*). Moreover, no significant differences were seen among fibrils or with different enzymes (Fig. 3). (*ii*) The diffusion constant of mutMMP-1 is the same on surface-attached fibrils (23) and fibrils suspended in a collagen gel (22). Because mutMMP-1 motion is dominated by binding at buckled sites (Fig. 2), buckle dynamics are likely comparable in attached and suspended fibrils.

Possible Origin of Internal Strain Energy

We have provided evidence for dynamic and spatially patterned molecular packing defects on the surface of collagen fibrils. In our model, strain energy stored in the fibril is relieved locally by an alternate conformation that involves reduced molecular packing constraints. Internal strain energy is consistent with increases in order and stability as fibrils form and are externally loaded. In solution, individual monomers are thermally unstable (32). Within a fibril, monomers are thermally stabilized by lateral packing (30), and the denaturation temperature increases with mechanical loading (33). Furthermore, monomers within native collagen have disordered regions, and disorder is reduced by applied tensile strain (34, 35).

Physiological Implications of Internal–Strain-Dependent Defect Formation in Fibrillar Collagen

Our data suggest that fibrillar collagen regulates its remodeling via the spontaneous formation of defect states that expose high-affinity MMP cleavage sites. In unloaded collagen fibrils, the "buckled" conformation exposes the otherwise protected (5), but thermally labile, MMP site (8, 32, 36, 37), creating an entry point for the initiation of proteolysis (23). Binding to the buckled site

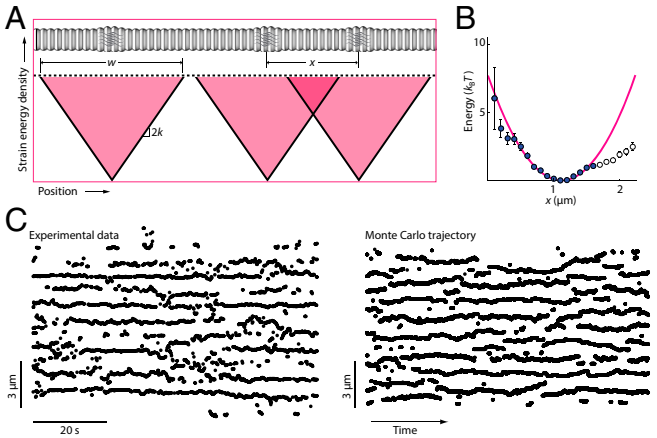

Fig. 5. Strain relief model recapitulates periodic and dynamic binding patterns in fibrillar collagen. (*A*) Buckles depicted as an alternate structural state in the fibril cartoon (top). The light pink shaded area between the dotted line (uniform strain energy density) and solid line (buckle strain energy density) is the strain energy relieved by formation of buckles. The distance over which the strain energy relief returns to the dotted line is the buckle width w, the distance between two buckles shown on the right is x, and the slope of the buckle strain energy density line is $2k$. The area of the dark pink shaded triangle, $[k(w - x)^2/2]$, is the increase in energy associated with two buckles separated by a distance $x < w$. (*B*) The binding site separation probability distribution $P(x)$ from Fig. 4*F* converted to an energy potential well through the relation, $P(x) \propto \exp[-k(x - \bar{x})^2/(2k_BT)]$. The energy was rescaled to zero at the center of the well. Filled data points were included in the fit of $P(x)$ (*Supporting Information*), returning estimates for the spring constant, $k = k_BT/\sigma^2$ (effective stiffness of the potential well), the average buckle separation, $\bar{x}$ (the potential well center spacing), and buckling energy, $\mu = k\bar{x}^2/2$. (*C*) Monte Carlo simulations (*Right*) of the model using the fitted parameters resemble experimental data (*Left*).

often occurs without subsequent cleavage but is an obligatory and rate-limiting step in the proteolysis of fibrillar collagen (23). An implication of this model is that degradation will be strongly inhibited by mechanical strain through a switch-like removal of buckle sites (16), consistent with the well-documented, but poorly understood, finding that fibrillar collagen under tension is resistant to degradation by MMP-1, MMP-8, and bacterial collagenase (15–17, 38–41). External tension on the fibril would decrease the internal strain energy that drives the formation of buckles. The model predicts that, once the uniform strain energy density (dotted line in Fig. 5*A*) decreases to the point that the strain energy relief per isolated buckle becomes smaller than μ, buckles cease to form and the fibril abruptly becomes resistant to degradation (Fig. S6). Such a mechanochemical switch has been observed by Flynn et al., who reported that strain inhibited degradation of tissue-derived fibrils by bacterial collagenase (16) and reconstituted fibrils by MMP-8 (15). There are conflicting reports on the effect of tension on enzymatic cleavage of isolated triple helices (42–44); however, these measurements are of uncertain significance with regard to natively assembled fibrils or collagen structures in tissues. Decisively, tension-dependent stabilization against MMP-1 has been demonstrated in native tissue (17).

Contractile forces of the cell, stresses exerted through changes during development, interstitial fluid pressure, and physical activity, alter the strain on fibrils and reinforce collagen in the direction of loading (45, 46). Our results indicate that external loading of collagen common to these processes inhibits the spontaneous formation of entry points, thereby limiting MMP accessibility. Spontaneous buckling may expose other cryptic sites in the fibril (47), including the fibronectin binding site through which collagen is connected to integrin and, through integrin, to the cell. Collagen provides the mechanical context for cells, influencing cellular identity and behavior, which, in turn, influence collagen remodeling (48, 49). The strain sensitivity of fibrillar collagen buckling provides a mechanistic basis for these observed reciprocal tensile interactions (50).

The internal strain we have identified in fibrillar collagen manifests in enzyme binding patterns with direct relevance to biological function. Microtubules and actin filaments are other examples of self-assembled load-bearing biological structures with the capacity to store energy within internally strained components, suggesting that enzyme recruitment to structurally altered sites might be a common tension-dependent regulatory mechanism. The underlying dynamic molecular changes in collagen structure, which may be on the order of single atoms (5), have evaded detection by conventional structural approaches but were readily observed through tracking of enzyme binding. This structure-through-binding technique could be extended to reveal molecular-scale features of other dynamical systems such as microtubules or actin filaments, which may similarly use internal strain to regulate enzyme binding and activity (51).

Methods

Preparing Collagen Fibrils and Matrix Metalloproteinase Enzymes. The methods for preparing MMP enzymes and the collagen fibril substrate have been described previously in detail (23). Briefly, we isolated type I collagen fibrils by mechanically abrading exposed rat tail tendon over an aldehyde-treated quartz microscope slide (CEL Associates Inc.). After washing away loose debris, including bundles of unbound fibrils, we immersed slides overnight at 4 °C in 50 mM Tris·HCl, pH 7.5, with 50 mM NaCl and 2 mg/mL BSA to block the surface against background enzyme adsorption.

We purified wild-type MMP-1, its active center disabled mutant, E219Q, and MMP-9 after transfection of their cDNAs in p2AHT2a cells, and then labeled the proenzyme by titrating either Alexa-488 or Alexa-555 fluorescent dye to obtain a final 1:1 ratio of label to enzyme. Immediately before an experiment, we activated the enzyme by incubation at 37 °C with 10:1 plasmin (MMP-9) or plasmin and stromelysin-1 (MMP-1) and, after 1 h, deactivated the plasmin with a fivefold molar excess of aprotinin. We verified the activity of labeled and unlabeled MMP-1 with reconstituted collagen fibrils. For all experiments, we used ~200 pM MMP in 50 mM Tris, pH 7.5 buffer including 150 mM NaCl and 1 mM $CaCl_2$. Measurements were performed at 20 °C except for the data presented in Fig. 3, which were obtained at 37 °C.

Nanodiamond Stabilized Single-Molecule Tracking of MMP Enzymes on Collagen Fibril Substrate. We recorded the motion of fluorescently labeled enzymes on intact, native type I collagen fibrils using prism-type total internal reflection microscopy with 532-nm laser excitation. The image was magnified at 167 nm per pixel onto an Andor DV897DCS-BV EMCCD camera, which captured 85 frames per second with a 10-ms exposure. To extract single-molecule trajectories from each 10,000-frame video file, we used the feature-point-based tracking software developed by the Mosaic group and provided as a free plugin in ImageJ (52–54). We set the following Mosaic tracking parameters: radius = 3, cutoff = 0, intensity = 1.0, range = 3, and distance = 2.7.

We corrected the measurement for stage drift by using a surface-immobilized fluorescent diamond (100-nm nominal diameter) as a stable reference point (55). To avoid adding high-frequency noise, we approximated the diamond trajectory with a smooth curve formed by linearly interpolating a series of 1,000-point Bezier curves at the adjoining vertices, and then subtracted the coordinates of the interpolated curve at each time point from every MMP trajectory. We fit a line to all MMP tracking points on a single fibril and applied a coordinate rotation using the fitted slope, thereby aligning (longitudinal) motion along the fibril and (lateral) motion across the fibril to orthogonal axes. To check the robustness of the correction for stage drift, we measured a second stationary diamond in the field of view: After correction, the measured diamond position changed by less than 30 nm after 20 min.

Origin of Periodicity in a Mechanical Buckling Model. We modeled the collagen fibril as a one-dimensional structure with internal strain, which is relieved locally by adoption of an alternate conformation that we call a "buckle." In a linear model (Fig. 5*A* and Fig. S4), the strain energy per unit length returns to baseline linearly over a distance $w/2$ to each side of the center of a buckle with a slope defined as $2k$. The strain energy stored in a segment of fibril is equal to the area under the strain-energy-per-unit-length curve. Hence, an isolated buckle reduces the internal strain energy by $kw^2/2$. If the distance between buckles decreases to less than w, the reduction in area under the strain-energy-per-unit-length curve is less than that for buckles separated by a distance exceeding w; the difference is equal to the area of overlap, $k(w-x)^2/2$. This dependence of energy on the separation, x, between buckles implies that they effectively repel each other when they come within a distance x less than w, with a force equal to $\mathrm{d}/\mathrm{dx}[k(w-x)^2/2] = k(w-x)$, and hence a spring constant k. If formation of an isolated buckle increases the energy by μ and reduces mechanical strain energy by $kw^2/2$, formation of a set of n buckles separated by distances x_i, $i = 1 \ldots n$, corresponds to a particular microstate with total energy $\Delta E = n(\mu - kw^2/2) + k/2\Sigma_i(w - x_i)^2 H(w - x_i)$, where H is a Heaviside function = 1 for $x_i < w$ and 0 otherwise. The Heaviside function imposes the condition that buckles closer to one another than w repulsively interact. The above model simplifies in a "mean field" approximation where buckles are evenly spaced ($x_i = L/n$ for all i), where L is the length of fibril containing n buckles. In this approximation, the total energy change is $\Delta E = n[\mu - kw^2/2 + k(w - L/n)^2/2]$. Minimizing ΔE with respect to n gives $\mu = k\bar{x}^2/2$, where $\bar{x} = L/n$.

Thermal Fluctuations: Variations in the Number and Spacing of Binding Regions. We performed a more detailed equilibrium model calculation assuming buckles are localized on a ring lattice of N sites. A ring was used so all interbuckle intervals could be treated equivalently. The energy of a set of n buckles with interbuckle spacings x_i is given by $E = n(\mu - kw^2/2) + k/2\Sigma_i(w - x_i)^2 H(w - x_i)$. Because $\sum x_i = L = N$ lattice units, a particular state (set of buckle positions) is equivalent to a "partition" of N into integers that sum to N. The "*IntegerPartitions*[*N*]" function in Mathematica creates a list of all partitions of an integer N. This function was used to create a list of all possible states of 1 to N buckles. The probability of a given energy state was assumed proportional to $\exp[-E(n,x_i)/(k_BT)]$. States with the same set of interbuckle spacings but arranged in different orders have the same energy. The number of such states for a given energy (the degeneracy of that energy state), $g(n, x_i)$, is given by $N!$ divided by the product of the factorials of the number of times each interbuckle spacing appears in the partition. Because the number of partitions of an integer N increases exponentially for large N, lattices were limited to $N \approx 35$ to keep the calculation time on the order of minutes on an Intel i7 processor. A canonical partition function $Q(L, k, w, n)$ was calculated in Mathematica as the sum of $g(n,x_i)\exp[-E(n,x_i)/(k_BT)]$ over all energy states with n buckles. A grand canonical partition function was calculated similarly as the sum over all energy states and all numbers of buckles: $Z(L, k, w) = \sum_{n=0}^{N} Q(L, k, w, n)$. In the thermodynamic limit, the expected number of buckles is $n^* = k_BT(\partial \ln Z/\partial\mu)_{L,T}$, and the probability of n buckles is $P(n) = Q(L, k, w, n)/Z(L, k, w)$ (56).

Monte Carlo Simulations of Mechanical Buckling Model. We represented the fibril as a one-dimensional lattice of length L with periodic boundary conditions and distance between lattice points much smaller than the average spacing between buckles. Starting with an arbitrary number and configuration of buckles, we used Mathematica to simulate the approach to an equilibrium distribution. The energy of each configuration of buckles at specified lattice points was calculated using E as before. Following Frenkel and Smit (57), at each simulation step, we randomly attempted to insert or delete a buckle with probability α, or move an existing buckle one lattice unit to the left or right with probability $1-2\alpha$, and accepted the change if the likelihood of the new state calculated from $P \propto \exp[-\Delta E/(k_B T)]$ exceeded a threshold whose value was chosen as a random number between 0 and 1. The results were insensitive to the choice of α and we typically set the attempt rates equal ($\alpha = 1/3$). After equilibrating the array for 5,000 steps, we plotted the buckle positions over the next 4,000 steps in the simulation (Fig. 5*C*). Such equilibrated trajectories are independent of the initial configuration or number of buckles in the starting array.

We estimated the number of simulation steps required to randomize buckle configurations by starting with two buckles at arbitrary positions, running the simulation until the number of buckles reached equilibrium (~10 buckles in ~500 simulation steps), and calculating the normalized spatial correlation between independently generated buckle configurations. Gaussians of equal amplitude and 0.12-μm SD were generated at each buckle position, and the Gaussians were summed to simulate histograms, $P(s, step)$, as in the calculation of experimental correlation times (*Supporting Information*). The spatial correlation between buckle positions in successive simulation steps decreased from 1 to the value of correlation between independent configurations after ~250 steps.

To calculate the distributions in the number and spacing of buckles (Fig. S5), we populated an ensemble of 1,000 uncorrelated buckle arrays by repeatedly equilibrating the system and recorded only the buckle configuration of the last step. The entire calculation ran efficiently (completed in minutes) for numbers of lattice points N up to a few hundred.

ACKNOWLEDGMENTS. We thank Hemai Parthasarathy and three anonymous referees for comments on the manuscript. This research was supported by the Intramural Research Program of the National Heart, Lung, and Blood Institute, National Institute of Arthritis and Musculoskeletal and Skin Diseases Grant R01AR040618, and National Cancer Institute Grant R01CA123363 (to G.G.).

1. Shoulders MD, Raines RT (2009) Collagen structure and stability. *Annu Rev Biochem* 78: 929–958.
2. Orgel JP, Irving TC, Miller A, Wess TJ (2006) Microfibrillar structure of type I collagen in situ. *Proc Natl Acad Sci USA* 103(24):9001–9005.
3. Sherman VR, Yang W, Meyers MA (2015) The materials science of collagen. *J Mech Behav Biomed Mater* 52:22–50.
4. Fields GB (2013) Interstitial collagen catabolism. *J Biol Chem* 288(13):8785–8793.
5. Perumal S, Antipova O, Orgel JP (2008) Collagen fibril architecture, domain organization, and triple-helical conformation govern its proteolysis. *Proc Natl Acad Sci USA* 105(8):2824–2829.
6. Van Doren SR (2015) Matrix metalloproteinase interactions with collagen and elastin. *Matrix Biol* 44-46:224–231.
7. Jackson BC, Nebert DW, Vasiliou V (2010) Update of human and mouse matrix metalloproteinase families. *Hum Genomics* 4(3):194–201.
8. Lu KG, Stultz CM (2013) Insight into the degradation of type-I collagen fibrils by MMP-8. *J Mol Biol* 425(10):1815–1825.
9. Gross J, Nagai Y (1965) Specific degradation of the collagen molecule by tadpole collagenolytic enzyme. *Proc Natl Acad Sci USA* 54(4):1197–1204.
10. Bonnans C, Chou J, Werb Z (2014) Remodelling the extracellular matrix in development and disease. *Nat Rev Mol Cell Biol* 15(12):786–801.
11. Humphrey JD, Dufresne ER, Schwartz MA (2014) Mechanotransduction and extracellular matrix homeostasis. *Nat Rev Mol Cell Biol* 15(12):802–812.
12. Page-McCaw A, Ewald AJ, Werb Z (2007) Matrix metalloproteinases and the regulation of tissue remodelling. *Nat Rev Mol Cell Biol* 8(3):221–233.
13. Malemud CJ (2006) Matrix metalloproteinases (MMPs) in health and disease: An overview. *Front Biosci* 11:1696–1701.
14. Nagase H, Visse R, Murphy G (2006) Structure and function of matrix metalloproteinases and TIMPs. *Cardiovasc Res* 69(3):562–573.
15. Flynn BP, et al. (2010) Mechanical strain stabilizes reconstituted collagen fibrils against enzymatic degradation by mammalian collagenase matrix metalloproteinase 8 (MMP-8). *PLoS One* 5(8):e12337.
16. Flynn BP, Tilburey GE, Ruberti JW (2013) Highly sensitive single-fibril erosion assay demonstrates mechanochemical switch in native collagen fibrils. *Biomech Model Mechanobiol* 12(2):291–300.
17. Lotz JC, Hadi T, Bratton C, Reiser KM, Hsieh AH (2008) Anulus fibrosus tension inhibits degenerative structural changes in lamellar collagen. *Eur Spine J* 17(9):1149–1159.
18. Murphy G, Nagase H (2008) Reappraising metalloproteinases in rheumatoid arthritis and osteoarthritis: Destruction or repair? *Nat Clin Pract Rheumatol* 4(3):128–135.
19. Nerenberg PS, Salsas-Escat R, Stultz CM (2007) Collagen—A necessary accomplice in the metastatic process. *Cancer Genomics Proteomics* 4(5):319–328.
20. Collier IE, Saffarian S, Marmer BL, Elson EL, Goldberg G (2001) Substrate recognition by gelatinase A: The C-terminal domain facilitates surface diffusion. *Biophys J* 81(4):2370–2377.
21. Collier IE, et al. (2011) Diffusion of MMPs on the surface of collagen fibrils: The mobile cell surface-collagen substratum interface. *PLoS One* 6(9):e24029.
22. Saffarian S, Collier IE, Marmer BL, Elson EL, Goldberg G (2004) Interstitial collagenase is a Brownian ratchet driven by proteolysis of collagen. *Science* 306(5693):108–111.
23. Sarkar SK, Marmer B, Goldberg G, Neuman KC (2012) Single-molecule tracking of collagenase on native type I collagen fibrils reveals degradation mechanism. *Curr Biol* 22(12):1047–1056.
24. Steele DL, et al. (2000) Expression, characterization and structure determination of an active site mutant (Glu202-Gln) of mini-stromelysin-1. *Protein Eng* 13(6):397–405.
25. Windsor LJ, Bodden MK, Birkedal-Hansen B, Engler JA, Birkedal-Hansen H (1994) Mutational analysis of residues in and around the active site of human fibroblast-type collagenase. *J Biol Chem* 269(42):26201–26207.
26. Ruggeri A, Benazzo F, Reale E (1979) Collagen fibrils with straight and helicoidal microfibrils: A freeze-fracture and thin-section study. *J Ultrastruct Res* 68(1):101–108.
27. Kleckner N, et al. (2004) A mechanical basis for chromosome function. *Proc Natl Acad Sci USA* 101(34):12592–12597.
28. Bowden N, Brittain S, Evans AG, Hutchinson JW, Whitesides GM (1998) Spontaneous formation of ordered structures in thin films of metals supported on an elastomeric polymer. *Nature* 393(6681):146–149.
29. Goehring L, Morris SW (2014) Cracking mud, freezing dirt, and breaking rocks. *Phys Today* 67(11):39–44.
30. Miles CA, Ghelashvili M (1999) Polymer-in-a-box mechanism for the thermal stabilization of collagen molecules in fibers. *Biophys J* 76(6):3243–3252.
31. Baldwin SJ, Quigley AS, Clegg C, Kreplak L (2014) Nanomechanical mapping of hydrated rat tail tendon collagen I fibrils. *Biophys J* 107(8):1794–1801.
32. Leikina E, Mertts MV, Kuznetsova N, Leikin S (2002) Type I collagen is thermally unstable at body temperature. *Proc Natl Acad Sci USA* 99(3):1314–1318.
33. Lennox FG (1949) Shrinkage of collagen. *Biochim Biophys Acta* 3(2):170–187.
34. Misof K, Rapp G, Fratzl P (1997) A new molecular model for collagen elasticity based on synchrotron X-ray scattering evidence. *Biophys J* 72(3):1376–1381.
35. Fraser RD, MacRae TP, Miller A (1987) Molecular packing in type I collagen fibrils. *J Mol Biol* 193(1):115–125.
36. Stultz CM, Edelman ER (2003) A structural model that explains the effects of hyperglycemia on collagenolysis. *Biophys J* 85(4):2198–2204.
37. Fields GB (1991) A model for interstitial collagen catabolism by mammalian collagenases. *J Theor Biol* 153(4):585–602.
38. Huang C, Yannas IV (1977) Mechanochemical studies of enzymatic degradation of insoluble collagen fibers. *J Biomed Mater Res* 11(1):137–154.
39. Nabeshima Y, Grood ES, Sakurai A, Herman JH (1996) Uniaxial tension inhibits tendon collagen degradation by collagenase in vitro. *J Orthop Res* 14(1):123–130.
40. Ruberti JW, Hallab NJ (2005) Strain-controlled enzymatic cleavage of collagen in loaded matrix. *Biochem Biophys Res Commun* 336(2):483–489.
41. Wyatt KE, Bourne JW, Torzilli PA (2009) Deformation-dependent enzyme mechanokinetic cleavage of type I collagen. *J Biomech Eng* 131(5):051004.
42. Camp RJ, et al. (2011) Molecular mechanochemistry: low force switch slows enzymatic cleavage of human type I collagen monomer. *J Am Chem Soc* 133(11):4073–4078.
43. Adhikari AS, Chai J, Dunn AR (2011) Mechanical load induces a 100-fold increase in the rate of collagen proteolysis by MMP-1. *J Am Chem Soc* 133(6):1686–1689.
44. Adhikari AS, Glassey E, Dunn AR (2012) Conformational dynamics accompanying the proteolytic degradation of trimeric collagen I by collagenases. *J Am Chem Soc* 134(32):13259–13265.
45. Shi Q, et al. (2014) Rapid disorganization of mechanically interacting systems of mammary acini. *Proc Natl Acad Sci USA* 111(2):658–663.
46. Bhole AP, Flynn BP, Liles M, Saeidi N, DiMarzio CA, JW Ruberti (2009) Mechanical strain enhances survivability of collagen micronetworks in the presence of collagenase: Implications for load-bearing matrix growth and stability. *Philos Trans R Soc A* 367(1902):3339–3362.
47. Orgel JP, et al. (2011) Collagen fibril surface displays a constellation of sites capable of promoting fibril assembly, stability, and hemostasis. *Connect Tissue Res* 52(1):18–24.
48. Levental KR, et al. (2009) Matrix crosslinking forces tumor progression by enhancing integrin signaling. *Cell* 139(5):891–906.
49. Trappmann B, et al. (2012) Extracellular-matrix tethering regulates stem-cell fate. *Nat Mater* 11(7):642–649.
50. Bissell MJ, Hall HG, Parry G (1982) How does the extracellular matrix direct gene expression? *J Theor Biol* 99(1):31–68.
51. Ehrlicher AJ, Nakamura F, Hartwig JH, Weitz DA, Stossel TP (2011) Mechanical strain in actin networks regulates FilGAP and integrin binding to filamin A. *Nature* 478(7368):260–263.
52. Chenouard N, et al. (2014) Objective comparison of particle tracking methods. *Nat Methods* 11(3):281–289.
53. Sbalzarini IF, Koumoutsakos P (2005) Feature point tracking and trajectory analysis for video imaging in cell biology. *J Struct Biol* 151(2):182–195.
54. Schindelin J, et al. (2012) Fiji: an open-source platform for biological-image analysis. *Nat Methods* 9(7):676–682.
55. Bumb A, Sarkar SK, Billington N, Brechbiel MW, Neuman KC (2013) Silica encapsulation of fluorescent nanodiamonds for colloidal stability and facile surface functionalization. *J Am Chem Soc* 135(21):7815–7818.
56. McQuarrie D (2000) *Statistical Mechanics* (Univ Sci, Sausalito, CA).
57. Frenkel D, Smit B (2002) *Understanding Molecular Simulation: From Algorithms to Applications* (Academic, San Diego).